Building Damage Visualization through Three-Dimensional Reconstruction Using Images and Point Clouds

Ittetsu Kuniyoshi [1], Sachie Sato [2], Yue Bao [1] , and Itsuki Nagaike [2]

[1] Department of informatics, Tokyo City University, Setagaya Campus, Tokyo 158-8557, Japan
[2] Department of architecture, Tokyo City University, Setagaya Campus, Tokyo 158-8557, Japan

Keywords: Architecture, remote sensing, 3D reconstruction, point cloud, sensor, visualization

Abstract

Assessing building damage caused by natural disasters, such as earthquakes and typhoons, involves an initial survey to measure wall inclination and determine risk levels. Traditional plumb line surveying methods can be influenced by external factors, such as wind and vibration, and require physical contact with the damaged buildings, posing a risk of collapse during the survey. This study proposes a method using a camera capable of simultaneously capturing three-dimensional (3D) point clouds and images. This method extracts the entire wall surface of a building through point cloud processing and calculates its inclination. In the experiments, the accuracy of the system was first verified using a simple storage shed, followed by validation of its effectiveness on an actual house. The results demonstrated that, compared with the conventional plumb line method, the proposed method could remotely measure the building without physical contact, ensuring the safety of surveyors. The proposed method achieved measurements with less error and provided a measurement accuracy comparable to or better than the plumb line method. The assessed inclination was used to determine the risk level of the wall surfaces, enabling an intuitive and visual evaluation by color-coding the entire wall surface according to the risk level.

1. INTRODUCTION

The causes of building damage are varied, encompassing not only natural wear and tear but also significant impacts from natural disasters such as typhoons and earthquakes. Following an earthquake, several assessments are conducted: the Emergency Safety Assessment, which aims to prevent secondary damage that could threaten human lives; the Damage Classification Assessment, which determines the long-term usability of affected buildings; and the Residential Damage Certification, which supports the issuance of disaster victim certificates. These assessment results have a direct impact on the usability of buildings, government assistance, and insurance payments, thus playing a crucial role in the lives of disaster survivors. The current emergency safety assessment relies mainly on visual inspection and simple tools, such as tape measures and plumb lines, to evaluate the exterior and measure building tilt. However, this method has limitations, as inspectors need to physically contact the building's first floor to take tilt measurements, which poses safety risks for inspectors and introduces variability due to reliance on their experience. For example, following the 2016 Kumamoto earthquake, it took approximately three weeks to complete most residential assessments. In densely populated areas like Setagaya and Ota wards, increasing the number of inspectors is challenging, making it difficult to conduct rapid assessments with the current method. Thus, there is a pressing need for a new, non-contact assessment method that reduces labor.

2. RELATED WORK

In recent years, three-dimensional measurement techniques utilizing 3D point cloud data, which eliminate the need for physical contact, have attracted attention. In the study by Hashikawa and Kanai, a method was proposed to automatically identify and extract standard steel structural members using point cloud data obtained from 3D laser measurements, specifically targeting structural components of steel bridges. Mishima, Kakizaki, and others applied plane detection to assess residual deformation and damage in reinforced concrete after loading, using 3D point cloud data collected with a laser profiler. However, this approach is limited to localized measurements of specific walls and cannot capture damage across an entire building’s wall surfaces. Asada and Hirakawa's research involved detecting edges on concrete wall surfaces using 3D point clouds to assess damage; however, this method relies solely on point cloud data, thus lacking the capability to confirm damage using images or video of the building. Deng and Dou’s research fused post-earthquake LiDAR data with aerial imagery to accurately analyze terrain changes and identify specific damage extents and severity. However, a key challenge with these approaches is that point cloud data captured from above makes it difficult to obtain detailed measurements on a building-by-building basis. Consequently, these methods are not yet suitable replacements for plumb line measurements currently used in the field.

This study proposes a method using Matterport, which can capture both 3D point cloud data and video simultaneously, to extract entire wall surfaces of buildings through point cloud processing and calculate tilt. Additionally, we evaluate damage conditions based on tilt for secondary structural components on wall surfaces in densely built-up residential areas. This approach enables a comprehensive and detailed assessment of building damage that was previously challenging with

conventional visual inspections and simple tools, proposing a method that directly reflects tilt levels onto building walls within video data, integrating wall surface evaluations with image data.

Figure 1. Earthquake-induced building damage

3. PROPOSED METHOD

3.1 Capturing building images and acquiring point cloud data

The scanning of point cloud data and photography are conducted using Matterport. Scan points are set at regular intervals around the building, and images are captured around the building to ensure visual overlap between each scan point. Matterport projects specific light patterns onto objects to acquire point cloud data. The captured image data and depth data are processed in Matterport's cloud, where the images and point cloud data are integrated.

3.2 Removal of unnecessary point clouds

First, the initial point cloud data is processed with RANSAC (RANdom SAmple Consensus) to identify the largest plane, which is assumed to be the floor. The point cloud data corresponding to this floor plane is then removed. RANSAC is a robust estimation method that mitigates the impact of outliers when determining planes. Fig. 3 illustrates the principle of RANSAC.

Figure 2. Floor removal

In environments such as residential areas, trees, utility poles, and power lines are present, making it necessary to perform clustering and filtering to remove unnecessary point cloud data.

3.3 Target building extraction process

A region-growing method was used to extract the point cloud data of a single building from the overall data. This method detects the main clusters from the entire point cloud dataset and extracts the point cloud with the largest cluster size, considering it to be related to the target building.

The region-growing method segments regions based on similarity criteria of surface normals and curvature within the point cloud.

When the angle between the normal vectors of two points falls below a specific threshold, they are grouped as part of the same structure, facilitating distinct segmentation of objects from the overall data. Each segmented cluster's point cloud size is evaluated, and the cluster with the largest size is identified as the target building. Point cloud data from other clusters are then removed.

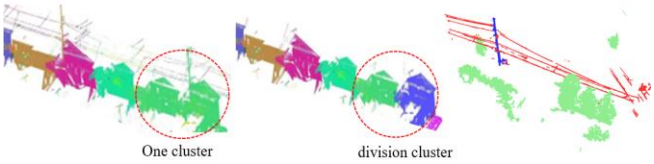

Figure 3. Obstacle removal using PCA and single building extraction using clustering"

In residential environments, obstacles such as hedges, utility poles, and power lines are present between adjacent buildings, necessitating clustering and filtering to remove unnecessary point cloud data. To identify these objects, it is essential to quantitatively represent the geometric features (such as planes, lines, and scattered shapes) underlying the point cloud data. Principal Component Analysis (PCA) is used to estimate fundamental quantities such as normals and curvature directly from the point cloud.

3.4 Extraction of major structural wall surfaces

The outer structure of a building typically consists of four large

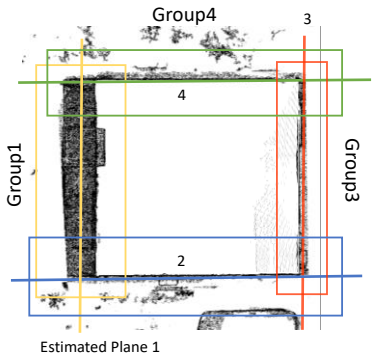

Figure 4. Wall surface extraction using RANSAC

wall surfaces. Each major wall point cloud invariably includes a large plane; thus, by grouping points within a certain width from the reference plane, the building point cloud can be segmented, allowing for the extraction of the primary wall surfaces. Given the measurement accuracy of the camera used in this study, which has a 1 cm error at 10 meters, a width of 3 cm was selected to capture 99.7% of the data within a range of 3σ based on a normal distribution.

3.5 Extract the corner parts of the wall by edge detection

To extract the planar surfaces at corner sections, which are the tilt measurement points, convex hull and point cloud interpolation are applied to the point cloud data extracted in step 2-3 (Figure 5). The convex hull represents the outer shape

of the point cloud and is well-suited for extracting corner sections. When forming the convex hull from the building's point cloud, the minimum and maximum points are used to define the corners, generating the main eight corner points.
The smallest convex hull containing the set of points

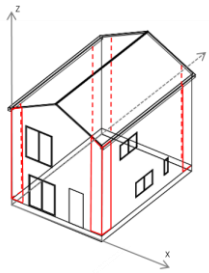

Figure 5. Corner extraction process

3.6 Point cloud 2D projection

Projection images of the building wall surfaces, along with depth images and coordinate data, are extracted. The projected images from each direction are used for matching with the camera images, as described later.

Figure 6. Projected 2D point cloud image

3.7 Window frame detection using 2D camera images

In this process, the extracted wall surface point cloud data is treated as images, and deep learning is used to identify window frames. Due to limitations in existing models for point cloud data, RGB images captured by Matterport are utilized instead.

Using homography transformation, the image with detected window frames is frontally aligned to facilitate matching with the projected point cloud images. This alignment allows for precise correspondence between the camera image and the 2D.

Figure7 . Wall frontalization via homography

3.8 Window area detection on point cloud projection images through matching

By aligning and matching the frontally transformed image with the point cloud projection images, window areas are detected directly on the projected point cloud. This process allows for accurate identification and extraction of window regions within the point cloud data, ensuring that structural details such as window frames are precisely mapped and localized within the 3D data representation.

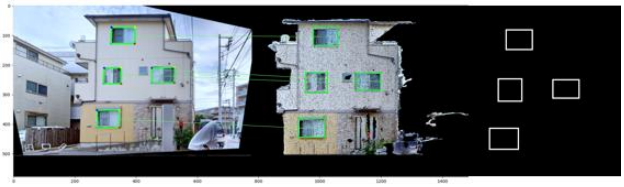

Figure 8 . Window region matching between camera image and projected point cloud

3.9 Calculation of wall surface inclination

For the point cloud extracted up to Section F, a plane is identified using RANSAC, and its inclination is calculated. Specifically, as depicted in Fig. 8, the normal vector of the estimated plane is determined. The angle between this normal vector and the horizontal plane vector is computed using Eq. (1), which represents the inclination of the wall surface. In Eq. (1), a, b, and c are the x, y, and z components of the plane's normal vector, respectively.

$$\theta = \arccos\left(\frac{c}{\sqrt{a^2 + b^2 + c^2}}\right) \qquad (1)$$

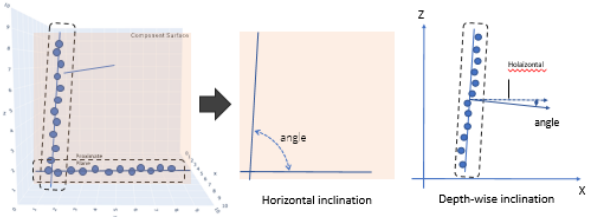

Figure 9. Line estimation and angle calculation

3.10 Visualization of risk

Angle of wall inclination		Classification
h = 1200 (mm)	$\theta = d/h$	
d ≦ 60	2.86 ° ≦ θ	Stable (case of reducing 50% in wind pressure)
20 < d ≦ 60	0.96 ° ≦ θ < 2.86 °	Assessment by other areas
d < 20	θ < 0.96 °	No assessment based on inclination

Table 1. Risk assessment based on inclination

To visually represent the degree of inclination of the building walls within the video, the extracted plane's point cloud is color-coded. This enables an intuitive display of the hazard level due to the building's tilt.
The method for displaying hazard levels using colors utilizes Eq. (2) to (4). In these Eq., "Hue" represents the hue in the HSV (Hue, Saturation, Value) color model, and "angle" denotes the inclination angle of the wall. The angle is linearly mapped to a specific range of hues to indicate different hazard levels.

Based on the "Operational guidelines for disaster-related residential damage certification criteria ," the relationship between color and hazard level is illustrated in the hazard determination table based on inclination below.

・Blue to Green Transition: Applied when angle ≤ 0.957°

$$\text{Hue} = 240 + \left(\frac{\text{angle}}{0.957}\right) \times (120 - 240) \quad (2)$$

・Green to Yellow Transition:

Applied when 0.957° ≦ angle ≦1.8°

$$\text{Hue} = 140 + \left(\frac{\text{angle} - 0.957}{1.8 - 0.957}\right) \times (90 - 120) \quad (3)$$

・Yellow to Red Transition: Applied when angle＞1.8°

$$\text{Hue} = 60 + \left(\frac{\text{angle}}{0.957}\right) \times (120 - 240) \quad (4)$$

Convert HSV color system hazards to RGB color system to display hazards as display images.
The final RGB values are obtained by adding the correction value m to each RGB component and scaling by 255.
Since the proposed system utilizes Matterport, the point cloud is meshed and converted into an object format to load the model assets. Finally, the hazard levels of the wall surfaces within the video are displayed using the Matterport SDK bundle

4. EXPERIMENT

To verify the effectiveness of the proposed method, four experiments were conducted.

Experimental 1

In Experiment 1, a small storage shed was selected as a simplified architectural model to confirm the basic effectiveness of the proposed method. The accuracy of detecting wall inclinations was evaluated, and a comparative verification was conducted with the plumb line method currently used in the field. Reference values were obtained using a digital angle meter, and the inclinations measured with the proposed method were compared with those from the plumb line method.

Experimental 2

To verify the applicability of the proposed method to actual residential buildings, we measured and compared its accuracy with the plumb line method on a detached house in a residential area. The practicality of the method was also assessed. Reference values were obtained using a digital angle meter, and the inclinations measured with the proposed method were compared with those from the plumb line method.

Experimental 3

An experiment is conducted to evaluate the risk when secondary structural components undergo deformation. Window frame detection is performed on point clouds of an actual residential building, followed by tilt measurement using a life-sized window frame model made of angled wood. This model simulates the deformation, allowing for precise assessment of the inclination and potential structural risk.

Experimental 4

We also examined one of the benefits of the proposed method: the intuitive hazard level display feature.

Experimental equipment

The equipment used in the experiments is described as follows:

Digital angle meter

・A digital angle meter was used as a reference tool to measure precise wall inclinations. It provides high-accuracy measurements used to validate results obtained from both the proposed method and the plumb line methods.

Plumb line

・Plumb line measurement method. A plumb line holder is attached to the wall, and the string
is extended vertically, achieving a length h of 120 cm from top to bottom. After the weight stops swinging, distances $d1$ and $d2$ from the top and bottom ends of the string to the wall are measured with a ruler. Using h, $d1$, and $d2$, the inclination I of the wall is calculated using (5).

$$I = \frac{d_1 - d_2}{h}. \quad (5)$$

Matterport Pro3

The 3D scanner Matterport Pro3 used for acquiring point cloud data. Its specifications are listed in Table 2.

Specification	Details
Product	Matterport Pro3
Camera Resolution	f20 megapixels 7680×4320
Accuracy	±20 mm (within 20 meters)
Scanning Range	Up to 50m
Field of View	360° horizontal, 300° vertical
Weight	1.78 kg
Dimensions	230 mm x 270 mm x 100 mm
Storage Capacity	32 GB internal

Table 2 . Camera used in the experiment

4.1 Verification using a storage shed

The subject used in this experiment is a storage shed measuring approximately 2.0 m in depth, 5.0 m in width, and 2.8 m in height, as depicted in Fig. 10.

Figure 10. Storage shed

The experimental procedure (a) ~ (c) is described below.

(a) As illustrated in Fig. 11, the camera was positioned approximately 2 m away from the wall, and images were captured at eight locations around the perimeter of the storage shed.

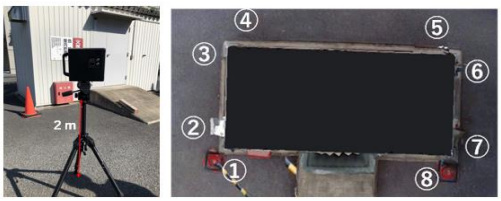

Figure 11. Shooting setup and shooting locations

(b) The point cloud data captured from the eight locations were integrated within Matterport. As shown in Fig. 12, the floor surface was first removed using RANSAC. Subsequently, segmentation was performed using the region-growing method to extract only the subject.

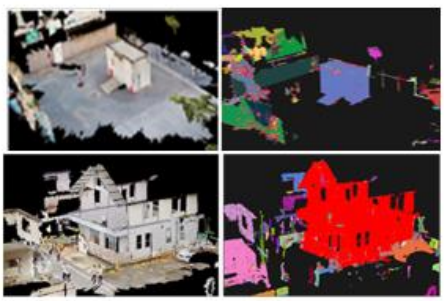

Figure 12. Preprocessing and segmentation

(c) To compare with the plumb line method, the corners of the extracted subject were identified using the convex hull from the point cloud data, as shown in Fig. 13.

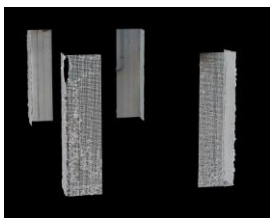

Figure 13. Corner extraction

4.2 Verification using a detached house

To verify the effectiveness of the proposed method in an actual residential setting, an experiment was conducted using a detached house in Ota City, Tokyo. The house, depicted in Fig. 14, measured approximately 9.3 m in depth, 8.3 m in width, and 5.4 m in height. Similarly, to reduce infrared interference from sunlight, the captures and point cloud acquisition were conducted in the evening. The weather conditions were cloudy. The total number of point cloud data points was 7,702,835, with a point spacing of approximately 0.01 m.
The experimental procedure (a) ~ (e) is described below.

Figure 13. Corner extraction

(a) The perimeter of the building was captured using the Matterport scanner.

(b) The point cloud data captured from the eight locations were integrated using Matterport's Cortex AI .

(c) Using RANSAC, the floor surface was removed, and segmentation was performed using the region-growing method to extract only the subject, as shown in Fig. 12.

The convex hull is the smallest convex shape that contains all the points in a plane or space. By performing this process, the shape that encloses the outer part of the given point cloud can be obtained. Therefore, edge detection was performed, as shown in Fig. 12, to extract only the wall surfaces by using the connections of the edges, as shown in Fig. 15(a). Subsequently, the convex hull was used to extract the corresponding points of the building's eight corners, as shown in Fig. 15(b). In the experiment, the point cloud data of the corners were extracted to match the 120 cm height range of the inclination survey conducted with the plumb line.

(d) The inclination of the wall surfaces at the extracted corners was calculated using (5) of the proposed method and compared with the inclination calculated using the plumb line method.
(e) To compare with the plumb line method, the corners of the

Figure 15. Point cloud data of corner sections.

building were extracted from the point cloud data using a convex hull, as shown in Fig. 15.

4.3 Detection of window frames in simplified models and residential point clouds

In this experiment, a life-sized model of a typical window frame was created, and inclination was introduced to the wooden frame and window frame to verify if the tilt could be accurately detected. This test aims to evaluate whether the tilt can be correctly measured even if deformation occurs in secondary components such as windows or doors during an earthquake.

First, the actual angle was measured using a digital protractor as a reference. The wooden model was constructed based on the standard dimensions of common window frames . The models used were the knee-wall type (07409) and the full-height type (16518), each following the typical dimensions of standard window frames.

Based on the standard dimensions of window sashes, life-sized sash models (hereafter referred to as "full-scale models") were created with actual dimensions (width W× height H) of 1690 × 1830 mm and 780 × 970 mm, as shown in Figure 2. The models were inclined at angles of 1/20 rad and 1/60 rad, which are the tilt thresholds used in emergency safety assessments after earthquakes. The experiment aimed to confirm whether these inclinations could be accurately detected. The tilt caused by construction errors due to sash dimensions is minimal and therefore considered negligible.

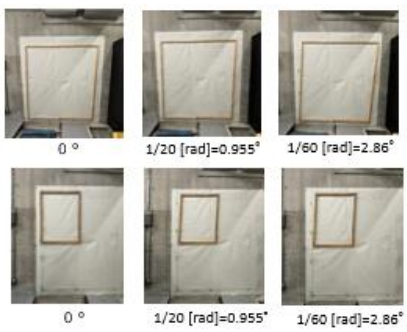

Figure 16. Shooting environment for window frame model

4.4 Visualization of hazard levels

As shown in Table 1 in Section 3.10, the disaster-related residential damage certification guidelines stipulate three hazard levels: no damage due to tilt, damage due to tilt, and red, respectively. This experiment verified whether the color coding accurately corresponds to these hazard levels.
Because real buildings typically do not exhibit inclinations within the range of all three hazard levels, an adjustable whiteboard was used to simulate different inclinations. As depicted in Fig. 17(a), the whiteboard was adjusted to three specific angles (0.05°, 1.15°, and 2.95°) corresponding to the three hazard levels. Inclined planes were created for this experiment.
The whiteboard used in the experiment has high rigidity and maintains a fixed angle to reduce the risk of unnecessary movement and measurement errors during the measurement process. The inclination angle is precisely measured using a digital angle meter, and by setting and fixing it to the exact angle, the setup closely replicates the conditions of measuring actual buildings.
Based on the inclinations calculated from the captured point cloud data, color coding was applied according to the hazard levels. Figs. 17(b), (c), and (d) show the results.
These results confirmed that the color coding accurately reflected the corresponding hazard levels.

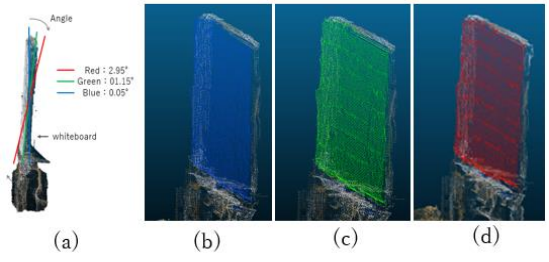

Figure 17. Color coding based on three angles.

5. RESULTS AND DISCUSSION

5.1 Experimental 1

Table 3 presents the experimental results, including average values, standard deviations, and mean errors of the inclinations obtained by comparing the proposed and traditional methods against the reference values.

Point	Standard value (°)	Average (°)		Standard deviation (°)		Mean error (°)	
		plumb bob	Proposed Method	plumb bob	Proposed Method	plum b bob	Proposed Method
1	-0.05	-0.0477	-0.0764	0.0642	0.0510	0.0023	0.0264
2	0.25	0.212	0.281	0.0696	0.0433	0.0423	0.0312
3	0.15	0.141	0.210	0.0520	0.0499	0.0091	0.0023
4	0.05	-0.0119	0.0249	0.0468	0.0517	0.0619	0.0251
5	0.1	0.0263	0.0841	0.0704	0.0692	0.0737	0.0159
6	-0.15	-0.105	-0.180	0.0455	0.0594	0.045	0.056
7	-0.1	-0.153	-0.0505	0.0700	0.0579	0.0528	0.0495
8	-0.1	-0.0597	-0.0770	0.0306	0.0564	0.0403	0.0597

Table 3 . Measurement Results of Experiment 1

Figure 18 illustrates the results of Table 2 in graphical form.
The errors of the proposed method were smaller than those of the plumb line method at locations 2, 3, 4, 5, and 7. Conversely, the errors of the proposed method were larger than those of the

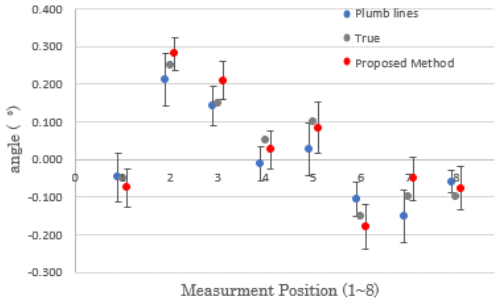

Figure 18. Comparison of the three sets of measurements.

plumb line method at measurement locations 1, 6, and 8.

Notably, the proposed method exhibited a maximum error of 0.0597° at measurement location 8, which remained lower than the 0.0737° error of the plumb line method.
The proposed method also showed smaller standard deviations than the plumb line method at locations 1, 3, 4, 5, and 7. However, at locations 2, 6, and 8, the proposed method had larger standard deviations compared to the plumb line method. In particular, at measurement location 6, the largest standard deviation of the proposed method (0.0692°) was within the largest measurement error of the plumb line (0.0704°).
Overall, comparing the proposed and plumb line methods across all eight locations revealed that the variability in measurements was either comparable or reduced with the proposed method, resulting in higher measurement accuracy.

5.2 Experimental 2

The inclination values obtained using the proposed method and the plumb line methods for the eight planes of the four extracted corners were compared with the reference values. The results are listed in Table 4.

Point	Standard value (°)	Average (°)		Standard deviation (°)		Mean error (°)	
		Plumb bob	Proposed Method	plumb bob	Proposed Method	plumb bob	Proposed Method
1	-0.05	0.0477	-0.0764	0.0642	0.0510	0.0023	0.0264
2	0.25	0.212	0.281	0.0696	0.0433	0.0423	0.03126
3	0.15	0.141	0.210	0.0520	0.0499	0.0091	0.0023
4	0.05	0.0119	0.0249	0.0468	0.0517	0.0619	0.0251
5	0.1	0.0263	0.0841	0.0704	0.0692	0.0737	0.0159
6	-0.15	-0.105	-0.180	0.0455	0.0594	0.045	0.056
7	-0.1	-0.153	-0.0505	0.0700	0.0579	0.0528	0.0495
8	-0.1	0.0597	-0.0770	0.0306	0.0564	0.0403	0.0597

Table 4. Measurement Results of experiment 2

Regarding relative errors compared to reference values, the proposed method had smaller errors than the plumb line method at five locations (1, 3, 6, 7, and 8), but larger errors at three locations (2, 4, and 5). At location 4, the proposed method had a maximum error of 0.123°, which was 0.021° greater than the plumb line method's 0.102°. However, at location 7, the proposed method's error was only 0.001° higher than the plumb line method's maximum of 0.124°, showing comparable results. At location 3, the plumb line method error was 0.1°, while the proposed method achieved a significantly smaller error of 0.001°.
The proposed method maintained accuracy even in areas like locations 3 and 7, where obstructions such as pipes were present. This indicates its ability to perform stable measurements despite noise, effectively removing obstacles like fences and pipes for accurate plane extraction. The proposed method's average error was 0.0604°, showing a 21.72% improvement over the traditional method's 0.0771°, confirming its enhanced measurement accuracy.
Overall, the proposed method showed equal or better performance compared to the plumb line method in real residential environments.

5.3 Experimental 3

Window areas were extracted from the acquired point cloud data, and sashes were extracted by plane detection.

Figure 19. Window frame point cloud extraction from building

The results indicate that the point cloud data allows for measurement of full-scale sash models of different sizes. Additionally, the successful extraction of not only the window area but also the sash components enables a more precise analysis of the sash condition. It was confirmed that evaluation can be performed for both horizontal tilt and depth-wise (longitudinal) tilt. This suggests that by measuring damage in three dimensions, the impact of earthquakes can be assessed in greater detail.

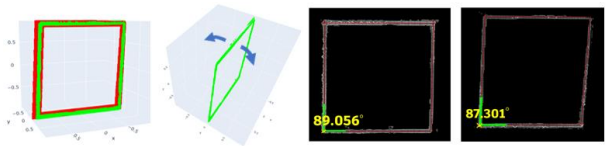

Figure 20. Inclination measurement of window frame model

5.4 Experimental 4

Based on the inclinations calculated from the point cloud data of the extracted corners in Experiments 1 and 2, color coding was applied according to the hazard levels of the emergency safety assessment. Fig. 21 shows the results.

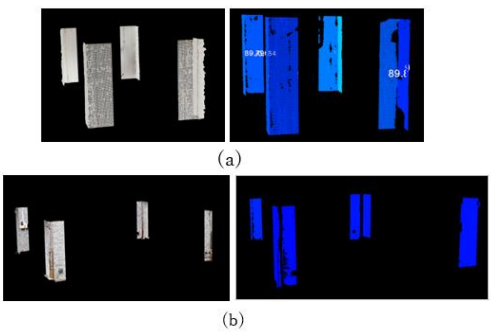

Figure 21. Hazard level display results.

All surfaces were color-coded as "no damage due to tilt," which was accurate since the examined buildings were currently used for storage and residential purposes.

To verify whether the hazard levels could be displayed in the video, the walls of the building were color-coded according to the hazard levels. Fig. 22 shows the results, confirming that the hazard levels of the entire wall surface could be intuitively confirmed.

Figure 22. Display of risk levels within the video.

6. Conclusion

In this study, we proposed a method that utilizes the Matterport
This study proposes a method using the Matterport 3D scanning camera to obtain 3D point cloud data of entire buildings, extract corner sections, and visualize hazard levels based on inclinations calculated with RANSAC. To verify its accuracy, experiments were conducted comparing it with the traditional plumb line method for measuring building tilt.
In the storage shed experiment, the proposed method showed smaller errors at five of the eight corners, with measurement variability reduced by 35.8% compared to the plumb line method. The maximum error was 0.0597°, about 19% smaller than the plumb line's maximum error of 0.0737°. On average, the proposed method's error was 15% lower.
In the detached house experiment, the proposed method also had smaller errors at five out of eight corners. The maximum error was 0.123°, less than the plumb line's 0.124°. Even where corner pipes or outdoor units were present, the proposed method showed comparable or lower errors. The overall average error was 21.72% smaller, confirming similar or better accuracy than the plumb line method.

Additional tests using life-sized window sash models with simulated inclinations showed that the proposed method accurately detected both horizontal and depth-wise tilt, effectively assessing complex deformations. This suggests it can provide detailed 3D evaluations of earthquake-induced damage, surpassing the limits of conventional 2D techniques.

The key features of the proposed method are summarized as follows:

1. Color-coded hazard levels: Allows for quick visual assessment.
2. Visual evaluation: Uses image and video data for enhanced assessment beyond numerical measurements.
3. Remote measurement: Enables safe, contactless building measurement.
4. Improved accuracy: Achieves results comparable to or better than the plumb line method in both real and simulated tests.
5. 3D deformation analysis: Offers comprehensive 3D evaluation of structural deformations, ideal for post-earthquake damage assessment.

Reference

General Incorporated Foundation Japan Building Disaster Prevention Association, 2017: Post-disaster building safety evaluation manual. *Japan Building Disaster Prevention Association*, Tokyo, Japan.

Cabinet Office, 2022: Operational guidelines for damage assessment criteria of houses affected by disasters. Available online: https://www.bousai.go.jp/taisaku/pdf/r303shinshin_all.pdf (accessed: 2022-10-01).

Japan Non-Life Insurance Association, 2022: Earthquake insurance damage survey: Criteria for damage assessment of earthquake insurance. Available online: https://www.sonpo.or.jp/insurance/jishin (accessed: 2022-10-01).

Fujiwara Sangyo, 2023: Plumb lines. Available online: https://www.fujiwarasangyo-markeweb2.com (accessed: 2023-05-22).

Hashikawa, M., Kanai, S., Date, H., 2017: Automatic extraction of steel bridge members based on laser-scanned point clouds. *Japan Society of Precision Engineering*, XLII-2/W7, 29-36.

Mishima, N., Sonzaki, K., 2019: Damage analysis of disaster-affected buildings using a surface characterization technique with three-dimensional point clouds. *Electrical and Information Related Societies, Kyushu Branch*, Tech. Rep. DOI: https://doi.org/10.11527/jceeek.2019.0_196.

Xin, Z., Asada, H., Gyotoku, N., 2017: A study on a method of making drawings of damage situation after the earthquake using 3D point cloud data of reinforced concrete buildings. *Geographic Information Systems Society of Japan*, 26, B-5-4.

Deng, F., Dou, A. X., Wang, X. Q., 2018: Fusion of aerial imagery and airborne LiDAR data for post-earthquake building point extraction. *Journal of Remote Sensing*, 22, 224-232.

Li, L., Yang, F., Zhu, H., Li, D., Li, Y., Tang, L., 2017: An improved RANSAC for 3D point cloud plane segmentation based on normal distribution transformation cells. *Remote Sensing*, 9, 433.

Rabbani, T., Van Den Heuvel, F., Vosselman, G., 2006: Segmentation of point clouds using smoothness constraint. *International Archives of Photogrammetry, Remote Sensing and Spatial Information Sciences*, 36, 248-253.

Ahmed, S. M., Tan, Y. Z., Chew, C. M., Mamun, A. A., Wong, F. S., 2018: Edge and corner detection for unorganized 3D point clouds with application to robotic welding. *IEEE/RSJ International Conference on Intelligent Robots and Systems*, XLII-2/W7, 29-36.

Murakami, K., Masuda, H., 2009: A study on smooth surface reconstruction from large-scale noisy point-clouds (1st report) - smoothing operators based on robust estimate. *Japan Society of Precision Engineering Autumn Conference*, 910.